Biotite as a recorder of an exsolved Li-rich volatile phase in upper-crustal silicic magma reservoirs

B.S. Ellis, J. Neukampf, O. Bachmann, C. Harris, F. Forni, T. Magna, Oscar Laurent, P. Ulmer

GEOLOGY | THE GEOLOGICAL SOCIETY OF AMERICA®

https://doi.org/10.1130/G49484.1

Manuscript received 7 July 2021
Revised manuscript received 29 October 2021
Manuscript accepted 31 October 2021

Published online 3 February 2022

Biotite as a recorder of an exsolved Li-rich volatile phase in upper-crustal silicic magma reservoirs

B.S. Ellis[1], J. Neukampf[1,2], O. Bachmann[1], C. Harris[3], F. Forni[4], T. Magna[5], O. Laurent[1,6] and P. Ulmer[1]

[1]Institute of Geochemistry and Petrology, ETH Zürich, CH-8092, Zurich, Switzerland
[2]Centre de Recherches Pétrographiques et Géochimiques, CNRS, 15 rue Notre Dame des Pauvres BP 20, F-54500 Vandœuvre les Nancy, France
[3]Department of Geological Sciences, University of Cape Town, 13 University Avenue, Rondebosch 7701, South Africa
[4]Department of Earth Sciences "Ardito Desio", University of Milan, via Mangiagalli 34, 20133 Milan, Italy
[5]Czech Geological Survey, CZ-11821 Prague, Czech Republic
[6]Géosciences Environnement Toulouse, CNRS, Observatoire Midi-Pyrénées, F-31400 Toulouse, France

ABSTRACT

The magmatic-hydrothermal transition is key in controlling the fate of many economically important elements due to the change in partitioning when melt and magmatic fluid coexist. Despite its increasing economic importance, the behavior of lithium (Li) in such environments remains poorly known. We illustrate how compositionally unusual biotites from the rhyolitic Bishop Tuff (California, USA) and Kos Plateau Tuff (Greece) may contain a magmatic volatile phase trapped between layers of biotite crystals. Despite originating in pristine deposits and showing the expected X-ray diffraction spectra, these biotites return low (<95 wt%) analytical totals via electron microprobe (EMP) consistent with the presence of considerable amounts of light elements (non-measurable by EMP). Lithium contents and isotope ratios in these biotites are remarkable, with abundances reaching >2300 ppm, exceptionally light Li isotopic compositions (δ^7Li as low as –27.6‰), and large isotopic fractionation between biotite and corresponding bulk samples ($\Delta^7Li_{bt-bulk}$ as low as –36.5‰). Other mineral phases, groundmass glass, and melt inclusions from the same units do not support an extremely Li-rich melt prior to eruption. Biotites from phonolitic systems (Tenerife [Canary Islands] and Campi Flegrei [Italy]) do not show such extreme compositional differences, with biotite and melt showing roughly equivalent Li contents, underscored by significantly reduced $\Delta^7Li_{bt-bulk}$ to a maximum of –10.9‰. We ascribe the difference in behavior to the near-liquidus appearance of biotite in alkaline magmatic suites, before widespread exsolution of a magmatic volatile phase in the magma reservoir, while in rhyolitic suites, biotite crystallizes at low temperature, trapping the coexisting exsolved fluid phase in the reservoir.

THE MAGMATIC-HYDROTHERMAL TRANSITION

The 'Green Revolution' to address current global climate change, and growing demand for energy storage in batteries (e.g., for electric vehicles) have focused attention on the occurrence and global cycling of the elements required for this technology, such as lithium, cobalt, or tellurium. Although lithium (Li) found in economic deposits is generally thought to be sourced from silicic magmatism (Hofstra et al., 2013; Benson et al., 2017; Ellis et al., 2021), the actual mechanisms by which Li is enriched and ultimately removed from these magmas remain poorly constrained. Many economically important metals are concentrated by processes such as partitioning between silicate melt and magmatic fluids occurring at the magmatic-hydrothermal transition; therefore, understanding these processes has been a topic of intense interest from both experimental perspectives (e.g., Webster et al., 2004; Iveson et al., 2019) and natural samples (Zajacz et al., 2008). Most studies of natural materials have focused on quartz-hosted melt and fluid inclusions. However, these studies require samples in which both inclusion types were synchronously trapped, which is rare in nature (Fiedrich et al., 2020), and are complicated by the diffusivity of many phases through their host minerals, which can modify initial concentrations (e.g., Audétat et al., 2018). We investigated the mineral biotite as a recorder of the magmatic-hydrothermal transition in a suite of samples from rhyolitic and phonolitic magmas. Specifically, we focused on the abundance and isotopic composition of Li in biotites from the rhyolitic Bishop Tuff (California, USA) and Kos Plateau Tuff (Greece) previously inferred to contain magmatic fluids (Hildreth, 1977; Bachmann, 2010). These biotites yield low electron microprobe totals (<95 wt%) and are hereafter termed "low-total biotites" (LTBs). For comparison, we also investigated biotites that yielded normal (95–97 wt%) analytical totals (hereafter abbreviated to NTBs) from a rhyolitic system with involvement of cumulate melts (Caetano Tuff, Nevada, USA; Watts et al., 2016) and alkaline suites (Astroni pyroclastics and Campanian Ignimbrite from the Campi Flegrei, Italy [Forni et al., 2018] and the Granadilla ignimbrite from Tenerife, Canary Islands [Bryan, 2006]).

METHODS

Pure biotite fractions were separated from bulk samples by crushing and handpicking under a binocular microscope. For *in situ* mineral analysis (all carried out at the Institute of Geochemistry and Petrology, ETH Zürich, Switzerland), biotites and groundmass glasses were embedded in epoxy, polished, and carbon coated prior to imaging using a JEOL JSM-6390 scanning electron microscope (SEM). Following imaging, samples were analyzed using JEOL JXA 8200 and 8230 Superprobe electron microprobes with conditions similar to those reported by Neukampf et al. (2019) for groundmass glass and biotites analyzed with operating conditions of 15 kV, 15 nA, and a 10 μm spot. Laser ablation–inductively coupled plasma–mass spectrometry (LA-ICPMS) trace elemental analyses were car-

CITATION: Ellis, B.S., et al., 2022, Biotite as a recorder of an exsolved Li-rich volatile phase in upper-crustal silicic magma reservoirs: Geology, v. 50, p. 481–485, https://doi.org/10.1130/G49484.1

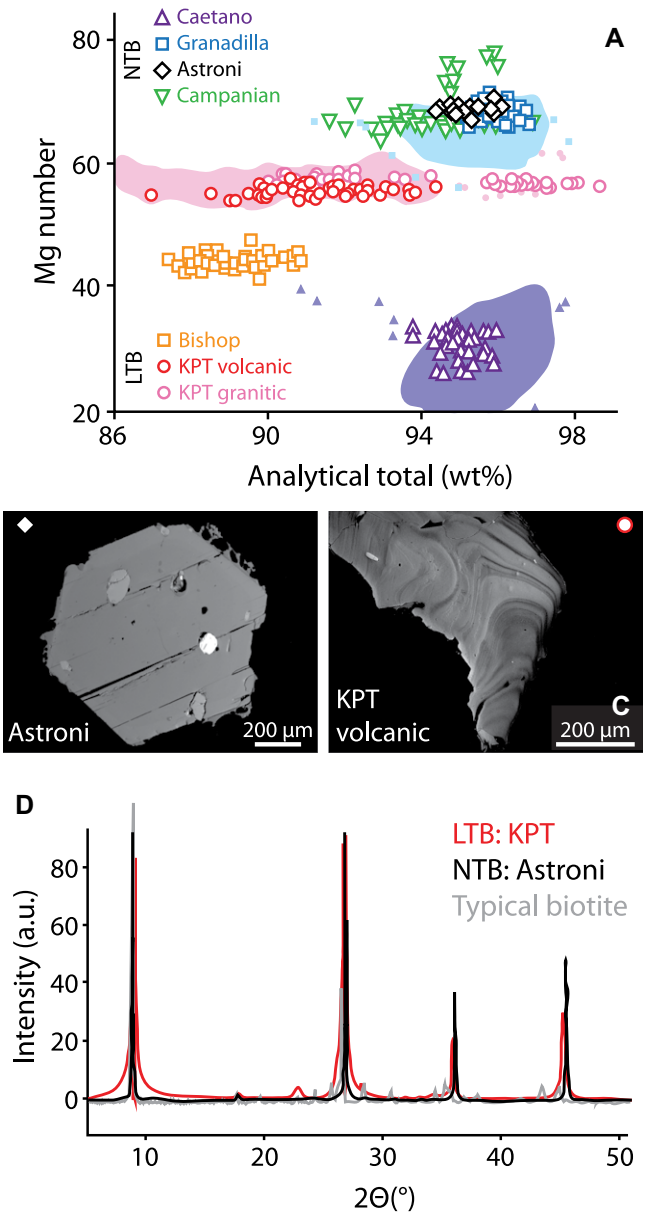

Figure 1. Biotite compositional and structural data. (A) Analytical totals of biotites shown against magnesium number [Mg# = 100 × molar Mg/(Mg + Fe)]. Literature data for the Caetano (Nevada, USA; Watts et al., 2016), Granadilla (Tenerife, Canary Islands; Bryan, 2006), and Kos (Greece; Bachmann, 2010) systems are shown for comparison in pale colors. NTB—normal-total biotite; LTB—low-total biotite; KPT—Kos Plateau Tuff. (B,C) Appearance of biotites from Astroni pyroclastics (Campi Flegrei, Italy) (NTB) and Kos Plateau Tuff (LTB) deposits illustrating different textures observed in backscattered electron imaging. (D) X-ray diffraction spectra of different biotites showing no other phases are included, with peak heights shown as arbitrary units (a.u.). Example biotite is sample R04144 from the RRUFF database (https://rruff.info).

ried out following the methods of Neukampf et al. (2021). In addition to the traditional spot analyses, we performed rastering analyses to minimize the depth of ablation.

For bulk-mineral analyses, crystal separates were isolated from the bulk-rock samples, milled, and then analyzed with X-ray diffraction (XRD) using an AXS D8 Advance diffractometer equipped with a Lynxeye superspeed detector at the Institute of Geochemistry and Petrology, ETH Zürich. Oxygen isotope analyses were performed at the University of Cape Town (South Africa) using conventional analyses on bulk samples of 50–100 mg and laser fluorination for biotites following the methods described by Ellis et al. (2021). Lithium isotopic measurements were carried out at the Czech Geological Survey in Prague (Czech Republic) following methods outlined in Magna et al. (2004). Different aliquots of the same samples (picked material and full dissolution) were analyzed to ensure the robustness of the results. Final values are expressed relative to the standard reference material for Li isotopes, L-SVEC, with the analytical uncertainty better than 0.5‰ (2 s.d. [standard deviation]). All new data from this study, as well as the results from reference materials, are provided in the Supplemental Material[1].

BIOTITE APPEARANCE AND COMPOSITION

Biotite from all samples lacks visible alteration in hand specimens and under the binocular microscope. In backscattered electron imaging, the LTBs have distinctly swirly textures with irregular zones of brightness, while the NTBs are typically homogeneous (Fig. 1). Our data (Fig. 1) agree well with those of previous studies for both LTBs (Kos Plateau Tuff [KPT]) and NTBs (Caetano Tuff). In contrast to previous studies (Bachmann, 2010), we did not observe the high Na_2O (to values >3 wt%) in LTBs from the KPT, but damage to biotite crystals is observable following microprobe analysis. Structural measurements using XRD reveal near-identical patterns between the NTBs and LTBs and indicate no additional crystalline or alteration phases are present. The broadening of the peaks in the LTB samples is consistent with a less structurally coherent biotite and consistent with the lower K + Na (a.p.f.u.[atoms per formula unit]) in the LTBs (Fig. S1 in the Supplemental Material). These data together with O isotopic compositions that indicate high-temperature equilibrium (Bachmann, 2010) argue against post-eruptive processes (e.g., Ellis et al., 2018) being responsible for the LTB compositions (Fig. S2).

LITHIUM SYSTEMATICS

Bulk-rock Li contents are unremarkable (Fig. S3), ranging from 10.7 to 33.3 ppm, and are unrelated to the biotite type (LTB versus NTB). The Li abundances of the groundmass glasses range from 2 to 70 ppm, with the highest values observed in the Astroni samples that contain NTBs and no relationship between groundmass Li content and biotite type (Fig. 2).

The Li contents of the LTBs are high, with the Kos samples ranging between 106 and 293 ppm (pumice) and between 180 and 510 ppm (granitic block) while the Bishop Tuff LTBs range from 848 to 2314 ppm. The elevated Li abundances in the LTBs were tested by both traditional point analyses and by rastering the laser across the biotite surfaces to minimize the depth effect of ablation. These methods yielded identical results (Fig. S4) without a clear relationship between biotite appearance and Li content. Bishop Tuff LTBs also contain elevated Cs (as much as 78 ppm), a feature previously interpreted as indicative of fluid involvement (Hildreth, 1977). In contrast, the NTB samples have significantly lower Li abundances (typically <25 ppm across the four NTB suites) and a more restricted range (Fig. 2A). The elevated Li contents in the LTBs are accompanied by remarkably low δ^7Li, as low as −27.6‰ and never exceeding −18.3‰, while the NTB samples have δ^7Li between −9.5‰ and 0.7‰ (Fig. 3). Within the KPT suite, the δ^7Li of volcanic and granitic samples varies in bulk rocks by ~7.5‰ and in biotites by ~7‰, which may reflect the different degassing regimes of these samples and highlight the complexity of Li studies in the magmatic environment. The $\Delta^7Li_{bt-bulk}$ (the difference between the δ^7Li values of biotite and bulk rock) ranges from −18‰ to

[1]Supplemental Material. Supplemental Figures S1–S8 (additional compositional information relevant to this study), and a supplemental dataset (all new data for this study and reference materials). Please visit https://doi.org/10.1130/GEOL.S.17264996 to access the supplemental material, and contact editing@geosociety.org with any questions.

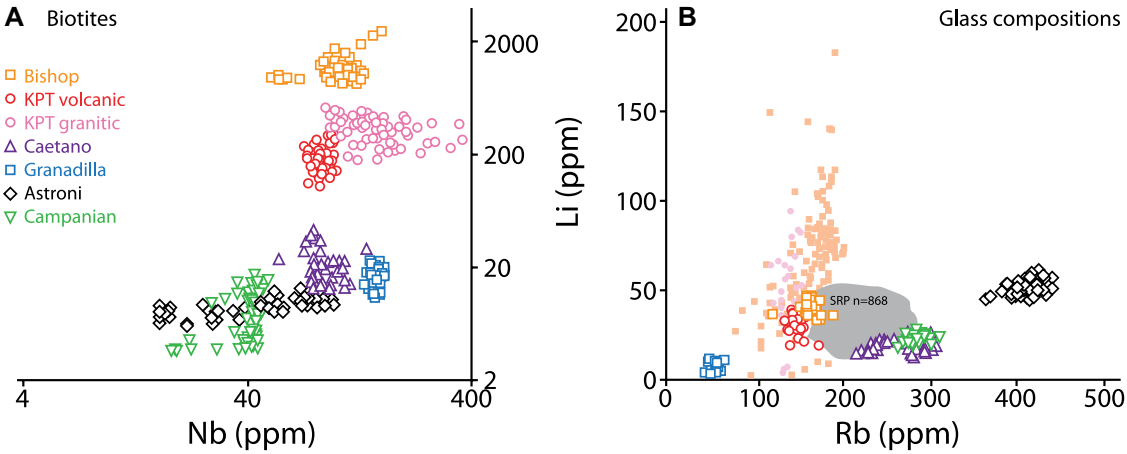

Figure 2. Lithium contents of biotites and coexisting groundmass glasses. (A) Biotite compositions from low-total biotites (LTBs) showing highly enriched Li contents (note logarithmic scale). Campi Flegrei (Italy) data are from this study and Forni et al. (2018). KPT—Kos Plateau Tuff. (B) Groundmass glasses illustrating that LTBs do not coexist with strongly Li-enriched melts. The field of Snake River Plain (SRP; western North America) glasses in gray from Ellis et al. (2021) indicates typical Li contents of rhyolitic glasses. Also shown in pale colors are melt inclusion compositions from the Bishop Tuff (Dunbar and Hervig, 1992; Wallace et al., 1999; Myers et al., 2019) and Kos Plateau Tuff (Bachmann et al., 2009).

−36.5‰ in the LTBs, while it is ∼−10‰ at maximum in the NTB units (Fig. 3A).

NO EVIDENCE FOR LITHIUM-ENRICHED MELTS

With lithium thought to be lost from the melt during syn-eruptive degassing (Neukampf et al., 2021), melt inclusions may have the potential to constrain the Li content of the melt prior to eruption. In the Bishop Tuff melt inclusions (Dunbar and Hervig, 1992; Wallace et al., 1999; Myers et al., 2019; Fig. 2B), Li and H_2O contents broadly covary while showing little relationship to Rb contents (Fig. S5), suggesting that Li may be lost through the host quartz following entrapment. Considering only inclusions with water contents >5 wt% (i.e., minimally degassed), the average Li content is 86.2 ± 30.2 ppm (n = 63, 1 s.d.) with a maximum of 206 ppm. Melt inclusions from the KPT are within a similar range, emphasizing that the systems producing the LTBs did not contain extremely Li-enriched melts prior to eruption (Fig. S5).

BIOTITE AS A FLUID TRAP

Although the Li abundance and δ^7Li values of the LTBs are extreme compared to those of the NTBs, it is noteworthy that previous studies have suggested that fluids exsolved from silicic magmas (Richard et al., 2018; Fiedrich et al., 2020) and pegmatites (Teng et al., 2006; Fan et al., 2020) trend toward high Li contents and low δ^7Li. In pegmatites, Fan et al. (2020) interpreted the ranges of Li abundances and isotopic ratios as resulting from melt-fluid separation whereby the Li-rich pegmatites were generated in a H_2O-rich and silicate-poor system; they proposed that ^{7}Li was enriched in the more strongly bonded residual melt while ^{6}Li was preferentially removed into the fluid. We argue that a similar process occurs in the LTBs, entrapping a Li-rich fluid preferentially residing between the biotite layers. Such a scenario explains the fragility of the LTBs under the microprobe beam, the unusual geochemistry, and the lack of readily visible fluid inclusions in conventional imaging. Bivariate plots of biotite compositions with Li (as a proxy of fluid involvement) against other elements are intriguing (Fig. S6). The variable behavior of elements of different geochemical affinities (e.g., potentially fluid-mobile elements such as Na, K, and Rb and those likely to be immobile such as La) indicates the complexity of fluid-melt-crystal partitioning in silicic magmatic systems and warrants further scrutiny.

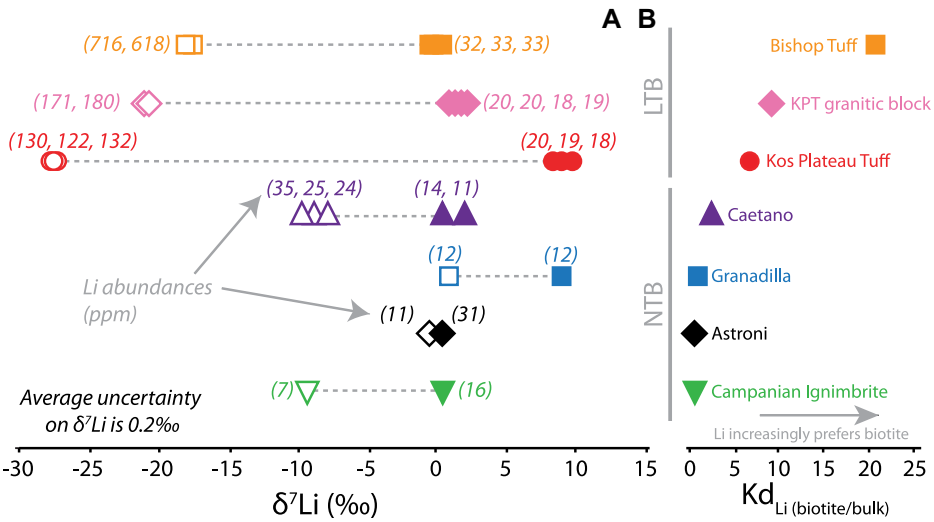

Figure 3. Lithium isotopic compositions. (A) Biotite (open symbols) and bulk-rock (filled symbols) δ^7Li values showing extremely low δ^7Li of low-total biotites (LTBs). NTB—normal-total biotite. Values in parentheses reflect Li abundance of sample. (B) Apparent partition coefficient (Kd) values calculated from dissolution inductively coupled plasma–mass spectrometry data showing the dramatic change in LTB samples. KPT—Kos Plateau Tuff.

RHYOLITES VERSUS PHONOLITES

Although medium- to low-K silicic magmas may or may not contain LTBs, such behavior has not been observed from high-K alkaline suites. In alkaline suites, biotite is typically a near-liquidus phase, as experimentally shown for Tenerife phonolites in which it may be the liquidus phase (Andújar et al., 2008). At Campi Flegrei, biotite is recognized as a high-temperature phase in magmatic evolution (Stock et al., 2016; Forni et al., 2018; Fig. 4A). Indeed, we note that the results from the Astroni pyroclastics and Campanian Ignimbrite samples are characteristic of the biotite-glass relationship in the Campi Flegrei, and data from 14 other deposits show similar features both for groundmass and biotite Li contents (Fig. S8).

In contrast, in medium- to low-K magmatic suites, biotite crystallizes much closer to the solidus, if at all. In a suite of water-saturated experiments (diamonds and dotted line in Fig. 4B) using a medium-K Adamello batholith (Italy) tonalite as starting material, Marxer and Ulmer (2019) showed biotite appearance at ∼750 °C. To further investigate this behavior, we used rhy-

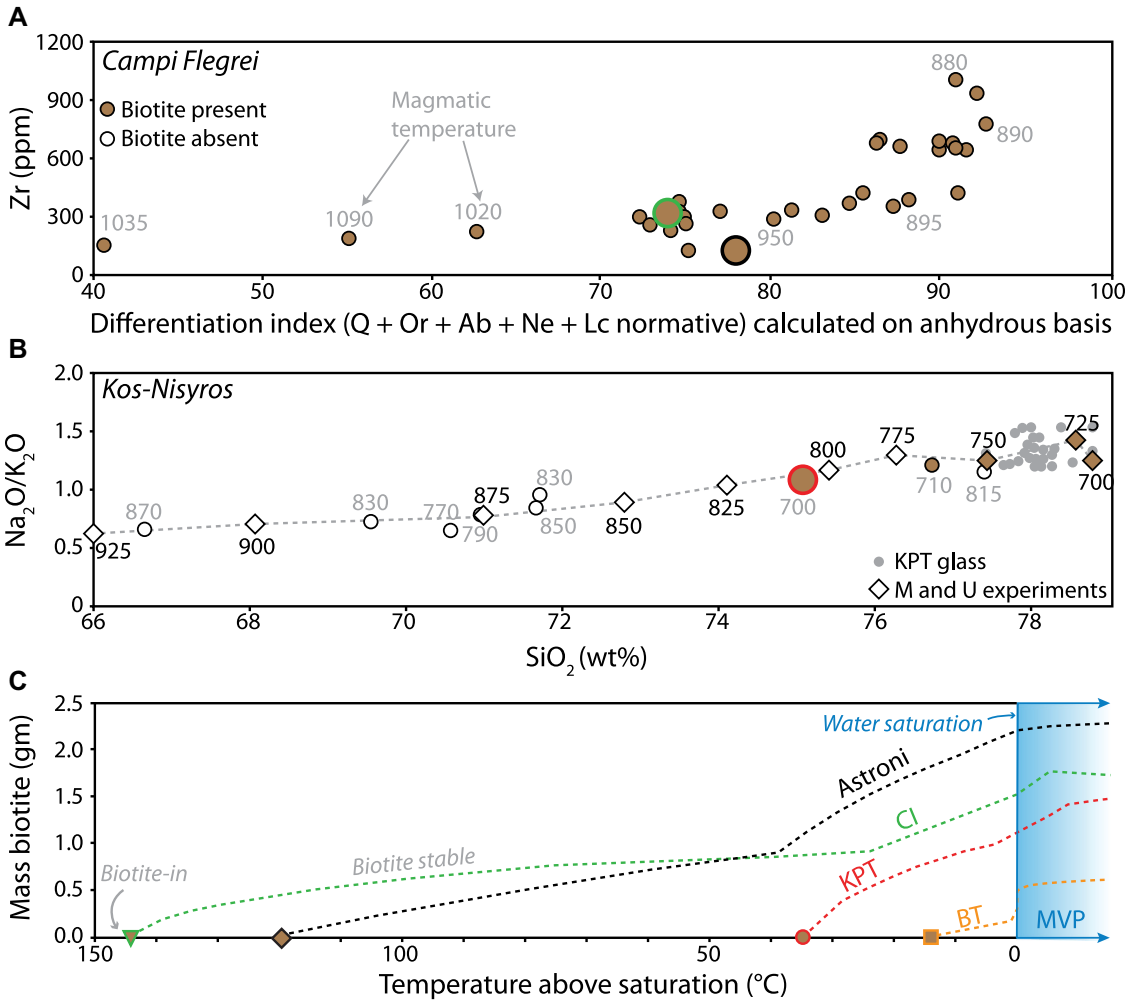

Figure 4. Bulk-rock evolution in Campi Flegrei (Italy) (A) and Kos-Nisyros (Greece) (B) systems, with symbol fill reflecting biotite occurrence. Larger symbols are samples from this study. Numbers reflect magmatic temperatures; in panel A, this is the lowest clinopyroxene-melt temperature (±20 °C), and in B, this is plagioclase-amphibole (±40 °C) or Fe-Ti oxide (±20 °C) thermometry with data from Bachmann et al. (2012), Forni et al. (2018), and Popa et al. (2019). Diamonds and dotted line in B illustrate experimental melt compositional evolution with experimental temperatures in black ("M and U experiments"; Marxer and Ulmer 2019) and biotite appearance at ~750 °C. Q—quartz, Or—orthoclase, Ab—albite, Ne—nepheline, Lc—leucite. (C) Rhyolite-MELTS models of systems with low-total biotite (LTB) and normal-total biotite (NTB) showing that in LTB systems, biotite predominantly crystallizes in the presence of magmatic volatile phase (MVP), while in NTB systems, it crystallizes mostly prior to exsolution of MVP. CI—Campanian Ignimbrite (Campi Flegrei, Italy); KPT—Kos Plateau Tuff (Greece); BT—Bishop Tuff (California, USA).

olite-MELTS modeling software (Gualda et al., 2012) to chart the relative appearances of biotite and a magmatic volatile phase (MVP) in magmatic systems containing the different biotite types (conditions for the models are provided in the Supplemental Material). As expected, in the alkaline suites, biotite appears at temperatures significantly (on the order 100–150 °C) above H_2O saturation (Fig. 4C). In the Caetano Tuff, melting of a sanidine-dominated cumulate (Watts et al., 2016) resulted in biotite crystallization from a drier, low-Mg# [Mg# = 100 × molar Mg/(Mg + Fe)], high-Ba melt (Fig. 1; Fig. S7) likely in the absence of a separate MVP. In the LTB-bearing systems, the biotite crystallization is delayed, which results in biotite crystallizing dominantly in the presence of an exsolved MVP (Fig. 4C). This illustrates the potential of biotite to capture such potentially Li-enriched fluids.

IMPLICATIONS

The record of Li-rich fluids trapped in pristine magmatic biotites from unmineralized, young volcanic deposits has important implications for the evolution of magmatic systems in the shallow crust and the transition from magmatic to hydrothermal conditions. First, the partitioning of Li into a MVP provides a mechanism to concentrate Li, and the fate of this MVP may be an important control on the generation of economic Li deposits as either brine deposits (Munk et al., 2016) or pegmatites (Troch et al., 2021). Second, the potential for biotites to contain "invisible" fluid inclusions between crystal layers may play a role in the occurrence of "too-old" $^{40}Ar/^{39}Ar$ ages that have previously been reported both from the Kos Plateau Tuff (Bachmann et al., 2010) and elsewhere (Hora et al., 2010). Finally, the LTBs can provide unambiguous evidence of the presence of an exsolved, compressible MVP in the magma reservoir, with major consequences for many magmatic processes including the size and styles of potential eruptions from such reservoirs (Huppert and Woods, 2002; Popa et al., 2019).

ACKNOWLEDGMENTS

We gratefully acknowledge generous funding from the Swiss National Science Foundation projects 200021_166281 and 200020_197040 to B.S. Ellis. T. Magna contributed through the Strategic Research Plan of the Czech Geological Survey (grant DKRVO/ČGS 2018–2022). We are extremely grateful for the generous assistance of Wes Hildreth and Kathryn Watts for helping with sampling the Bishop Tuff and sharing samples of the Caetano caldera ignimbrite, respectively. We thank Martin Mangler and Alex Iveson for their thoughtful reviews that helped improved this work, and Marc Norman for efficient editorial handling.

REFERENCES CITED

Andújar, J., Costa, F., Martí, J., Wolff, J.A., and Carroll, M.R., 2008, Experimental constraints on pre-eruptive conditions of phonolitic magma from the caldera-forming El Abrigo eruption, Tenerife (Canary Islands): Chemical Geology, v. 257, p. 173–191, https://doi.org/10.1016/j.chemgeo.2008.08.012.

Audétat, A., Zhang, L., and Ni, H., 2018, Copper and Li diffusion in plagioclase, pyroxenes, olivine and apatite, and consequences for the composition of melt inclusions: Geochimica et Cosmochimica Acta, v. 243, p. 99–115, https://doi.org/10.1016/j.gca.2018.09.016.

Bachmann, O., 2010, The petrologic evolution and pre-eruptive conditions of the rhyolitic Kos Plateau Tuff (Aegean arc): Central European Journal of Geosciences, v. 2, p. 270–305, https://doi.org/10.2478/v10085-010-0009-4.

Bachmann, O., Wallace, P.J., and Bourquin, J., 2009, The melt inclusion record from the rhyolitic Kos Plateau Tuff (Aegean Arc): Contributions to Mineralogy and Petrology, v. 159, p. 187–202, https://doi.org/10.1007/s00410-009-0423-4.

Bachmann, O., Schoene, B., Schnyder, C., and Spikings, R., 2010, The $^{40}Ar/^{39}Ar$ and U/Pb dating of young rhyolites in the Kos-Nisyros volcanic complex, Eastern Aegean Arc, Greece: Age discordance due to excess ^{40}Ar in biotite: Geochemistry Geophysics Geosystems, v. 11, Q0AA08, https://doi.org/10.1029/2010GC003073.

Bachmann, O., Deering, C.D., Ruprecht, J.S., Huber, C., Skopelitis, A., and Schnyder, C., 2012, Evolution of silicic magmas in the Kos-Nisyros volcanic center, Greece: A petrological cycle associated with caldera collapse: Contributions to Mineralogy and Petrology, v. 163, p. 151–166, https://doi.org/10.1007/s00410-011-0663-y.

Benson, T.R., Coble, M.A., Rytuba, J.J., and Mahood, G.A., 2017, Lithium enrichment in intracontinental rhyolite magmas leads to Li deposits in caldera basins: Nature Communications, v. 8, 270, https://doi.org/10.1038/s41467-017-00234-y.

Bryan, S.E., 2006, Petrology and geochemistry of the Quaternary caldera-forming, phonolitic Granadilla eruption, Tenerife (Canary Islands): Journal of Petrology, v. 47, p. 1557–1589, https://doi.org/10.1093/petrology/egl020.

Dunbar, N.W., and Hervig, R.L., 1992, Petrogenesis and volatile stratigraphy of the Bishop Tuff: Evidence from melt inclusion analysis: Journal of Geophysical Research, v. 97, p. 129–150, https://doi.org/10.1029/92JB00764.

Ellis, B.S., Szymanowski, D., Magna, T., Neukampf, J., Dohmen, R., Bachmann, O., Ulmer, P., and Guillong, M., 2018, Post-eruptive mobility of lithium in volcanic rocks: Nature Communications, v. 9, 3228, https://doi.org/10.1038/s41467-018-05688-2.

Ellis, B.S., Szymanowski, D., Harris, C., Tollan, P.M.E., Neukampf, J., Guillong, M., Cortes-Calderon, E.A., and Bachmann, O., 2021, Evaluating the potential of rhyolitic glass as a lithium source for brine deposits: Economic Geology, https://doi.org/10.5382/econgeo.4866 (in press).

Fan, J.J., Tang, G.J., Wei, G.J., Wang, H., Xu, Y.G., Wang, Q., Zhou, J.S., Zhang, Z.Y., Huang, T.Y., and Wang, Z.L., 2020, Lithium isotope fractionation during fluid exsolution: Implications for Li mineralization of the Bailongshan pegmatites in the West Kunlun, NW Tibet: Lithos, v. 352–353, 105236, https://doi.org/10.1016/j.lithos.2019.105236.

Fiedrich, A.M., Laurent, O., Heinrich, C.A., and Bachmann, O., 2020, Melt and fluid evolution in an upper-crustal magma reservoir, preserved by inclusions in juvenile clasts from the Kos Plateau Tuff, Aegean Arc, Greece: Geochimica et Cosmochimica Acta, v. 280, p. 237–262, https://doi.org/10.1016/j.gca.2020.03.038.

Forni, F., Degruyter, W., Bachmann, O., De Astis, G., and Mollo, S., 2018, Long-term magmatic evolution reveals the beginning of a new caldera cycle at Campi Flegrei: Science Advances, v. 4, eaat9401, https://doi.org/10.1126/sciadv.aat9401.

Gualda, G.A.R., Ghiorso, M.S., Lemons, R.V., and Carley, T.L., 2012, Rhyolite-MELTS: A modified calibration of MELTS optimized for silica-rich, fluid-bearing magmatic systems: Journal of Petrology, v. 53, p. 875–890, https://doi.org/10.1093/petrology/egr080.

Hildreth, E.W., 1977, The magma chamber of the Bishop Tuff: Gradients in temperature, pressure, and composition [Ph.D. thesis]: Berkeley, University of California, 328 p.

Hofstra, A.H., Todorov, T.I., Mercer, C.N., Adams, D.T., and Marsh, E.E., 2013, Silicate melt inclusion evidence for extreme pre-eruptive enrichment and post-eruptive depletion of lithium in silicic volcanic rocks of the western United States: Implications for the origin of lithium-rich brines: Economic Geology, v. 108, p. 1691–1701, https://doi.org/10.2113/econgeo.108.7.1691.

Hora, J.M., Singer, B.S., Jicha, B.R., Beard, B.L., Johnson, C.M., de Silva, S., and Salisbury, M., 2010, Volcanic biotite-sanidine $^{40}Ar/^{39}Ar$ age discordances reflect Ar partitioning and pre-eruption closure in biotite: Geology, v. 38, p. 923–926, https://doi.org/10.1130/G31064.1.

Huppert, H.E., and Woods, A.W., 2002, The role of volatiles in magma chamber dynamics: Nature, v. 420, p. 493–495, https://doi.org/10.1038/nature01211.

Iveson, A.A., Webster, J.D., Rowe, M.C., and Neill, O.K., 2019, Fluid-melt trace-element partitioning behaviour between evolved melts and aqueous fluids: Experimental constraints on the magmatic-hydrothermal transport of metals: Chemical Geology, v. 516, p. 18–41, https://doi.org/10.1016/j.chemgeo.2019.03.029.

Magna, T., Wiechert, U.H., and Halliday, A.N., 2004, Low-blank isotope ratio measurement of small samples of lithium using multiple-collector ICPMS: International Journal of Mass Spectrometry, v. 239, p. 67–76, https://doi.org/10.1016/j.ijms.2004.09.008.

Marxer, F., and Ulmer, P., 2019, Crystallisation and zircon saturation of calc-alkaline tonalite from the Adamello Batholith at upper crustal conditions: An experimental study: Contributions to Mineralogy and Petrology, v. 174, 84, https://doi.org/10.1007/s00410-019-1619-x.

Munk, L.A., Hynek, S.A., Bradley, D.C., Boutt, D., Labay, K., and Jochens, H., 2016, Lithium brines: A global perspective, *in* Verplanck, P.L., and Hitzman, M.W., eds., Rare Earth and Critical Elements in Ore Deposits: Reviews in Economic Geology, v. 18, p. 339–365, https://doi.org/10.5382/Rev.18.14.

Myers, M.L., Wallace, P.J., and Wilson, C.J.N., 2019, Inferring magma ascent timescales and reconstructing conduit processes in explosive rhyolitic eruptions using diffusive losses of hydrogen from melt inclusions: Journal of Volcanology and Geothermal Research, v. 369, p. 95–112, https://doi.org/10.1016/j.jvolgeores.2018.11.009.

Neukampf, J., Ellis, B.S., Magna, T., Laurent, O., and Bachmann, O., 2019, Partitioning and isotopic fractionation of lithium in mineral phases of hot, dry rhyolites: The case of the Mesa Falls Tuff, Yellowstone: Chemical Geology, v. 506, p. 175–186, https://doi.org/10.1016/j.chemgeo.2018.12.031.

Neukampf, J., Ellis, B.S., Laurent, O., Steinmann, L.K., Ubide, T., Oeser, M., Magna, T., Weyer, S., and Bachmann, O., 2021, Time scales of syn-eruptive volatile loss in silicic magmas quantified by Li isotopes: Geology, v. 49, p. 125–129, https://doi.org/10.1130/G47764.1.

Popa, R.-G., Bachmann, O., Ellis, B.S., Degruyter, W., Tollan, P., and Kyriakopoulous, K., 2019, A connection between magma chamber processes and eruptive styles revealed at Nisyros-Yali volcano (Greece): Journal of Volcanology and Geothermal Research, v. 387, 106666, https://doi.org/10.1016/j.jvolgeores.2019.106666.

Richard, A., Banks, D.A., Hendriksson, N., and Lahaye, Y., 2018, Lithium isotopes in fluid inclusions as tracers of crustal fluids: An exploratory study: Journal of Geochemical Exploration, v. 184, p. 158–166, https://doi.org/10.1016/j.gexplo.2017.10.017.

Stock, M.J., Humphreys, M.C.S., Smith, V.C., Isaia, R., and Pyle, D.M., 2016, Late-stage volatile saturation as a potential trigger for explosive volcanic eruptions: Nature Geoscience, v. 9, p. 249–254, https://doi.org/10.1038/ngeo2639.

Teng, F.Z., McDonough, W.F., Rudnick, R.L., and Walker, R.J., 2006, Diffusion-driven extreme lithium isotopic fractionation in country rocks of the Tin Mountain pegmatite: Earth and Planetary Science Letters, v. 243, p. 701–710, https://doi.org/10.1016/j.epsl.2006.01.036.

Troch, J., Huber, C., and Bachmann, O., 2021, The physical and chemical evolution of magmatic fluids in near-solidus silicic magma reservoirs: Implications for the formation of pegmatites: American Mineralogist, https://doi.org/10.2138/am-2021-7915 (in press).

Wallace, P.J., Anderson, A.T., and Davis, A.M., 1999, Gradients in H_2O, CO_2, and exsolved gas in a large-volume silicic magma system: Interpreting the record preserved in melt inclusions from the Bishop Tuff: Journal of Geophysical Research, v. 104, p. 20,097–20,122, https://doi.org/10.1029/1999JB900207.

Watts, K.E., John, D.A., Colgan, J.P., Henry, C.D., Bindeman, I.N., and Schmitt, A.K., 2016, Probing the volcanic-plutonic connection and the genesis of crystal-rich rhyolite in a deeply dissected supervolcano in the Nevada Great Basin: Source of the late Eocene Caetano Tuff: Journal of Petrology, v. 57, p. 1599–1644, https://doi.org/10.1093/petrology/egw051.

Webster, J., Thomas, R., Forster, H.-J., Seltmann, R., and Tappen, C., 2004, Geochemical evolution of halogen-enriched granite magmas and mineralizing fluids of the Zinnwald tin-tungsten mining district, Erzgebirge, Germany: Mineralium Deposita, v. 39, p. 452–472, https://doi.org/10.1007/s00126-004-0423-2.

Zajacz, Z., Halter, W.E., Pettke, T., and Guillong, M., 2008, Determination of fluid/melt partition coefficients by LA-ICPMS analysis of co-existing fluid and silicate melt inclusions: Controls on element partitioning: Geochimica et Cosmochimica Acta, v. 72, p. 2169–2197, https://doi.org/10.1016/j.gca.2008.01.034.

Printed in USA